Cellular and Molecular Bioengineering (2023) 16:355–367
https://doi.org/10.1007/s12195-023-00770-2

SI: 2023 CMBE YOUNG INNOVATORS

Bio-adhesive Macroporous Hydrogels for In Situ Recruitment and Modulation of Dendritic Cells

Joonsu Han[1] · Rimsha Bhatta[1] · Hua Wang[1,2,3,4,5,6,7]

Received: 23 February 2023 / Accepted: 14 June 2023 / Published online: 3 July 2023

Abstract

Introduction Biomaterials that enable in situ recruitment and modulation of immune cells have demonstrated tremendous promise for developing potent cancer immunotherapy such as therapeutic cancer vaccine. One challenge related to biomaterial scaffold-based cancer vaccines is the development of macroporous materials that are biocompatible and stable, enable controlled release of chemokines to actively recruit a large number of dendritic cells (DCs), contain macropores that are large enough to home the recruited DCs, and support the survival and proliferation of DCs

Methods Bio-adhesive macroporous gelatin hydrogels were synthesized and characterized for mechanical properties, porous structure, and adhesion towards tissues. The recruitment of immune cells including DCs to chemokine-loaded bioadhesive macroporous gels was analyzed. The ability of gels loaded with granulocyte-macrophage colony-stimulating factor (GM-CSF) and tumor extracellular vesicles (EVs) to elicit tumor-specific $CD8^+$ T cell responses was also analyzed.

Results Here we develop a bioadhesive macroporous hydrogel that can strongly adhere to tissues, contain macropores that are large enough to home immune cells, are mechanically tough, and enable controlled release of chemokines to recruit and modulate immune cells in situ. The macroporous hydrogel is composed of a double crosslinked network of gelatin and polyacrylic acid, and the macropores are introduced via cryo-polymerization. By incorporating GM-CSF and tumor EVs into the macroporous hydrogel, a high number of DCs can be recruited in situ to process and present EV-encased antigens. These tumor antigen-presenting DCs can then traffic to lymphatic tissues to prime antigen-specific $CD8^+$ T cells.

Conclusion This bioadhesive macroporous hydrogel system provides a new platform for in situ recruitment and modulation of DCs and the development of enhanced immunotherapies including tumor EV vaccines. We also envision the promise of this material system for drug delivery, tissue regeneration, long-term immunosuppression, and many other applications.

Keywords Extracellular vesicle · Cancer vaccine · Bioadhesive · Dendritic cell · Immunotherapy

Introduction

Cancer immunotherapy has reshaped the paradigm for cancer treatment in the clinic over the past decade, especially with the success of checkpoint blockades and chimeric antigen receptor (CAR) T cell therapies [10, 16, 26, 34]. However, the poor patient response rate, modest efficacy against solid tumors, and occasionally severe side effect have limited their utility and motivated the development of new immunotherapies that can elicit persistent cytotoxic T lymphocyte (CTL) response [13, 19, 32, 33]. Therapeutic cancer vaccines that aim to modulate antigen presenting cells (e.g., dendritic cells (DCs) with tumor antigens and adjuvants has shown the promise to elicit tumor-specific CTL response while exhibiting benign safety profiles, but are limited by the modest therapeutic efficacy [12, 21, 36, 38, 47]. To further improve the CTL response and antitumor efficacy, various types of neoantigen vaccines, tumor extracellular vesicle (EV) vaccines, DC vaccines, nanovaccines, and biomaterial scaffold-based vaccines have been actively explored [6, 7, 29, 39, 42]. Among them, chemokine-loaded biomaterial scaffolds such as poly(lactic-co-glycolic acid) scaffold, mesoporous silica rods, pore-forming alginate gels, and polymeric cryogels, upon administration, enable the active recruitment of DCs and subsequent modulation

Associate Editor Michael R. King oversaw the review of this article

Joonsu Han and Rimsha Bhatta have contributed equally to this work.

Extended author information available on the last page of the article

of DCs in situ. [3, 11, 44, 52] For example, the recruited DCs can be programmed by a pool of tumor antigens and adjuvants preloaded into the biomaterial scaffold, before migrating to the draining lymph nodes to prime antigen-specific $CD8^+$ T cells [2, 9]. One challenge related to biomaterial scaffold-based cancer vaccines is the development of macroporous materials that are biocompatible and stable, enable controlled release of chemokines to actively recruit a large number of DCs, contain macropores that are large enough to home the recruited DCs, and support the survival and proliferation of DCs [18].

Here report the use of a macroporous hydrogel system that fulfills these requirements and could provide a new platform for in situ recruitment and modulation of DCs and the development of robust cancer vaccines. Hydrogels composed of a robust gel network have demonstrated tremendous promise for hemostasis, drug delivery, wound healing, and other applications over the past several years [5, 17]. These hydrogels are mechanically tough and show great stability under physiological conditions. By incorporating amine-reactive *N*-hydroxysuccinimidyl (NHS) functional groups into the gel network, the hydrogels can also function as a bioadhesive by adhering to amine-bearing tissues [50]. The stable covalent linkage, together with the ability of the tough gel network to dissipate energy from the adhesion layer, resulted in strong and robust adhesion [14, 20, 41]. In this study, we utilized a cryo-polymerization process to introduce macropores (50–200 μm) into the gel network and thus fabricate macroporous hydrogels (Fig. 1). Further, chemokines such as granulocyte-macrophage colony-stimulating factor (GM-CSF) can be encapsulated into the macroporous hydrogel for controlled release and active recruitment of DCs [45, 46]. We envision that GM-CSF-loaded macroporous hydrogels, upon administration into the body, can adhere to the local tissue, retain at the administration site for a long period of time, and gradually release GM-CSF to recruit DCs. The recruited DCs can then become programmed within the hydrogel by antigens and adjuvants, prior to their migration to the draining lymph nodes for T and B cell priming. [1, 28]

To compose a functional cancer vaccine, tumor antigens also need to be incorporated into the GM-CSF-loaded macroporous hydrogel [23, 30]. Commonly used sources of tumor antigens include killed tumor cells, tumor cell lysates, tumor-derived EVs, and neoantigens [8, 35, 49]. Among them, killed tumor cells and tumor cell lysates are easy to obtain, but the variety of unknown components being released into the body often pose safety concerns [24]. Neoantigens that result from genetic mutation are relatively tumor-specific. However, the costly, lengthy, and lowly successful process of identifying neoantigens, which includes the isolation of tumor cells, extraction of DNAs or RNAs, sequencing, mutation analysis, epitope prediction, synthesis of a large pool of peptides, and screening of potential neoantigen candidates, has limited the development of neoantigen-based cancer vaccines [37, 51]. In contrast, tumor EVs, the nanosized extracellular vesicles secreted by tumor cells, exhibit a benign safety profile, are easy to isolate and purify, and have shown the promise to elicit tumor-specific

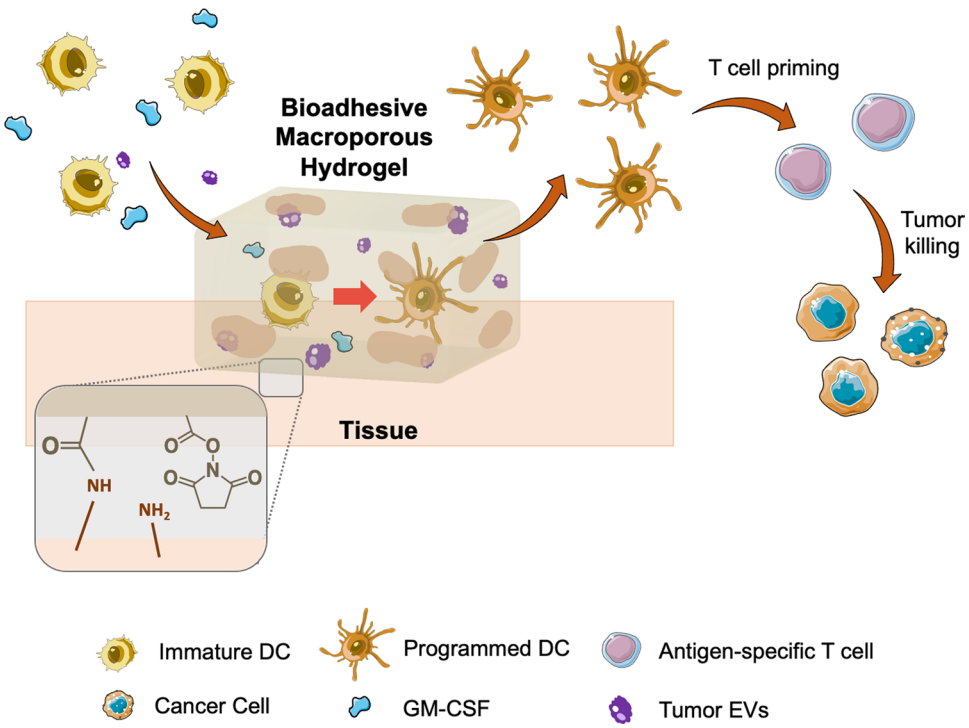

Fig. 1 Schematic illustration of bio-adhesive macroporous hydrogels for in situ recruitment and modulation of DCs. NHS-bearing gels can strongly adhere to tissues, while releasing GM-CSF to actively recruit DCs. The recruited DCs can then process and present EV-encased tumor antigens for subsequent priming of antigen-specific $CD8^+$ T cells

CTL response [22, 40, 43]. In this study, by co-encapsulating tumor EVs and GM-CSF into the bioadhesive macropoous hydrogel, DCs can be actively recruited to the material site to process and present EV-encased tumor antigens in situ, before they migrate to lymphatic tissues to prime antigen-specific $CD8^+$ T cells (Fig. 1).

Results

Synthesis and Characterization of Bioadhesive Macroporous Hydrogels

To synthesize the bioadhesive macroporous hydrogels, acrylic acid NHS ester, methacrylated gelatin, acrylic acid, and α-ketoglutaric acid (photoinitiator) were mixed and frozen at − 80 °C to form ice crystals between polymer chains, and then subjected to ultraviolet (UV) irradiation for 10 or 15 minutes (Fig. 2a). In this process, UV irradiation generated free radicals to initiate the co-polymerizatrion of acrylic

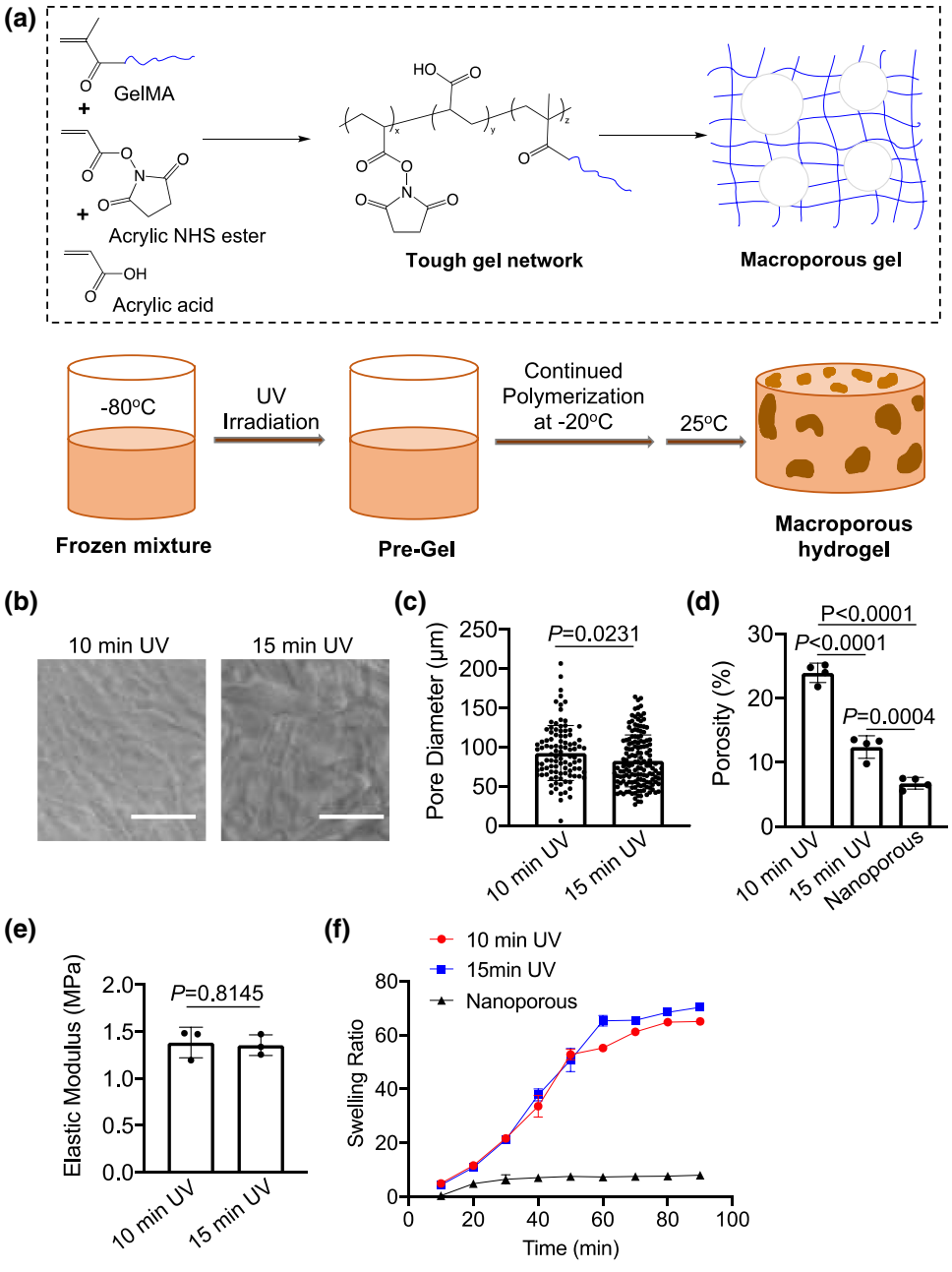

Fig. 2 Synthesis and characterization of macroporous hydrogels. **a** Schematic illustration and synthetic route of macroporous tough hydrogels. **b** Microscopic images of macroporous hydrogels with 10-min or 15-min UV irradiation. Scale bar: 150 μm. **c** Pore diameter of macroporous hydrogels. **d** Porosity of macroporus hydrogels. Nanoporous gels are used as the control. **e** Elastic modulus of the synthesized macroporus hydrogels. **f** Swelling of half-dried macroporous gels over time in PBS at 37 °C. All the numerical data are presented as mean ± SD ($0.01 < {}^*P \le 0.05$; ${}^{**}P \le 0.01$; ${}^{***}P \le 0.001$)

acid NHS ester, methacrylated gelatin, and acrylic acid. As the polymerization occurs within a fully frozen mixture, ice crystals were well dispersed within the formed gel network. By transferring to ambient temperature or 37 °C, the embedded ice crystals would melt and result in the formation of a macroporous gel network, as observed under the microscope (Fig. 2b). Quantification of microscopic images revealed an average diameter of 92 μm for 10-min UV irradiation and 83 μm for 15-min UV irradiation (Fig. 2c). These macropores are large enough to accommodate DCs and other immune cells with a diameter of ~ 10 μm. The porosity of the formed macroporous hydrogels can also be tuned by the UV irradiation time, with a porosity of 24.9% for 10-min UV irradiation (Fig. 2d). By increasing the UV irradiation time to 15 min, the porosity of gels decreased to 12.4% (Fig. 2d). It is noteworthy that despite the presence of interconnected macropores, the fabricated gels have a high elastic modulus of ~ 1.4 MPa (Fig. 2e), indicating the superior mechanic strength of the formed macroporous gels. When immersing the half-dried macroporous gel in PBS at 37 °C, the gel can rapidly swell with a much higher swelling ratio than conventional nanoporous hydrogels (Fig. 2f), further confirming the interconnected macroporous structure and the high mechanical strength of the gel network.

Bio-adhesive Property of Macroporous Hydrogels

The NHS-bearing macroporous hydrogels are expected to covalently conjugate to amine-bearing tissues while the robust gel network is able to dissipate energy from the interface, resulting in the formation of a stable adhesion layer. To assess the adhesive property, macroporous gels ($24 \times 24 \times 0.25$ mm) were placed between two pieces of porcine skin, and the adhesion strength was characterized via a peeling test on an Instron. The peeling test revealed an adhesion energy (interfacial toughness) of ~ 480 J/m^2 for the macroporous hydrogel, which is significantly higher than the control gel without NHS moieties (~190 J/m^2) and the commercial surgical sealant Dermabond (~ 60 J/m^2) (Fig. 3a–c). We also measured the shear strength of gels via a lap-shear

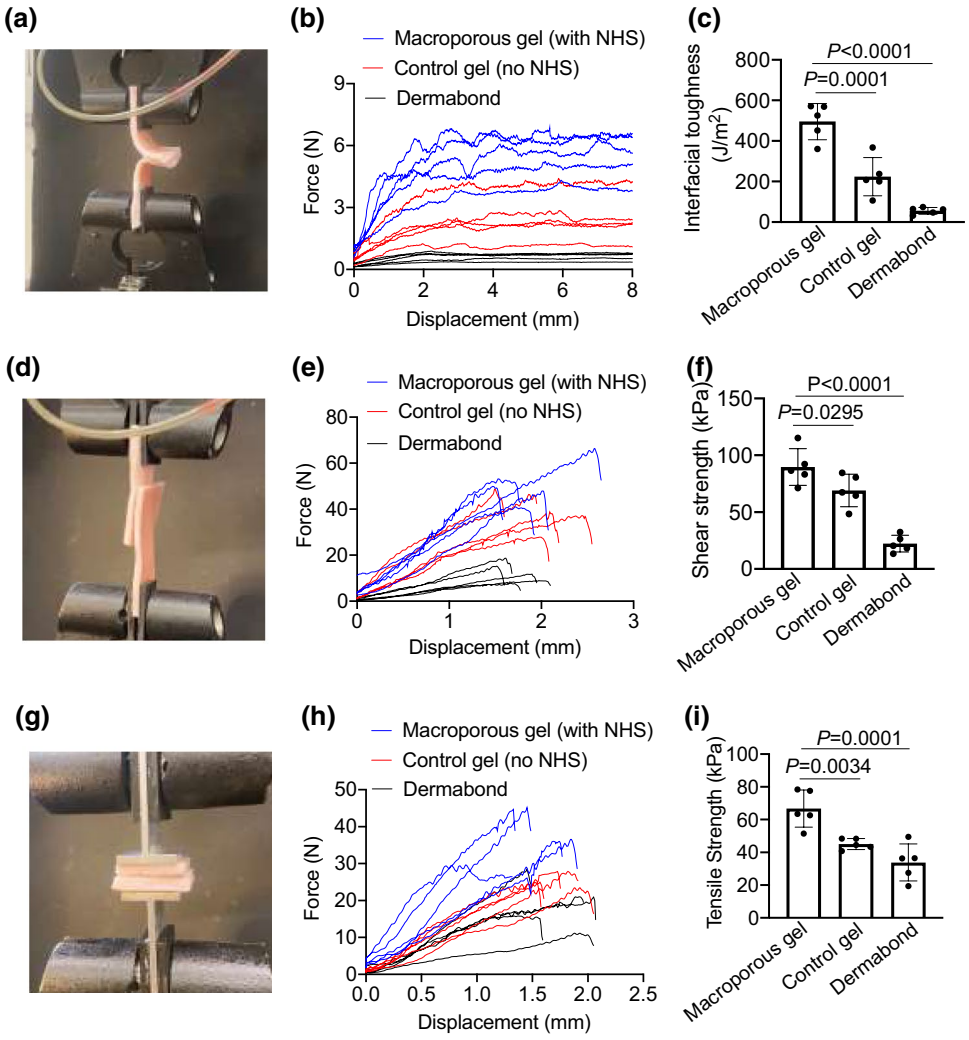

Fig. 3 Bioadhesive properties of macroporous hydrogels. **a** pictures illustrating the peeling test with porcine back skin. **b** Force–displacement profiles and **c** interfacial toughness of gels towards porcine skin. **d** pictures illustrating the lab-shear test with porcine back skin. **e** Force–displacement profiles and **f** shear strength of gels towards porcine skin. **g** pictures illustrating the tensile test with porcine back skin. **h** Force–displacement profiles and **i** tensile strength of gels towards porcine skin. All the numerical data are presented as mean ± SD ($0.01 < {*}P \le 0.05$; ${**}P \le 0.01$; ${***}P \le 0.001$)

test (Fig. 3d). The macroporous hydrogels showed a shear strength of 90 kPa (Fig. 3e–f), which was again higher than the control gel without NHS moiety and Dermabond. Similarly, tensile tests showed a tensile strength of 67 kPa for the macroporous hydrogel, in comparison with 45 kPa for control gels without NHS moiety and 34 kPa for Dermabond (Fig. 3g–i). These experiments demonstrated that our NHS-bearing macroporous hydrogels can strongly adhere to tissues.

Cell Infiltration and Survival in Macroporous Hydrogels

We next tested the biocompatibility and cell infiltration efficiency of the macroporous hydrogel. A small volume of EL4 cells in DMEM (1.5 million cells in 10 µL of DMEM) were added to the top of the macroporous hydrogel (6 mm in diameter and 0.25 mm in height). Cells could easily infiltrate into the gel and reach a loading efficiency of ~ 60% (Fig. 4a). The loading efficiency decreased with the initial cell density, as expected (Fig. 4b). Nevertheless, over 1 million cells can be easily loaded into a thin macroporous hydrogel (6 mm in diameter and 0.25 mm in height). The loaded EL4 cells showed good viability over time, as evidenced by the fluorescence images of cells on days 3, 5, and 8 after staining with Calcein AM (live cell stain) and Ethidium Homodimer-1 (dead cell stain) (Fig. 4c and d). Cells also showed good proliferation within the gels over time. These experiments demonstrated the good biocompatibility of the macroporous hydrogel which supports the survival and proliferation of loaded or infiltrated cells.

EV-Loaded Gels for DC Modulation In Vitro

After demonstrating that cells can be easily loaded into the macroporous hydrogel and survive well within the gels, we next incorporated tumor EVs into the gel and studied whether DCs can process and present EV-encased antigens

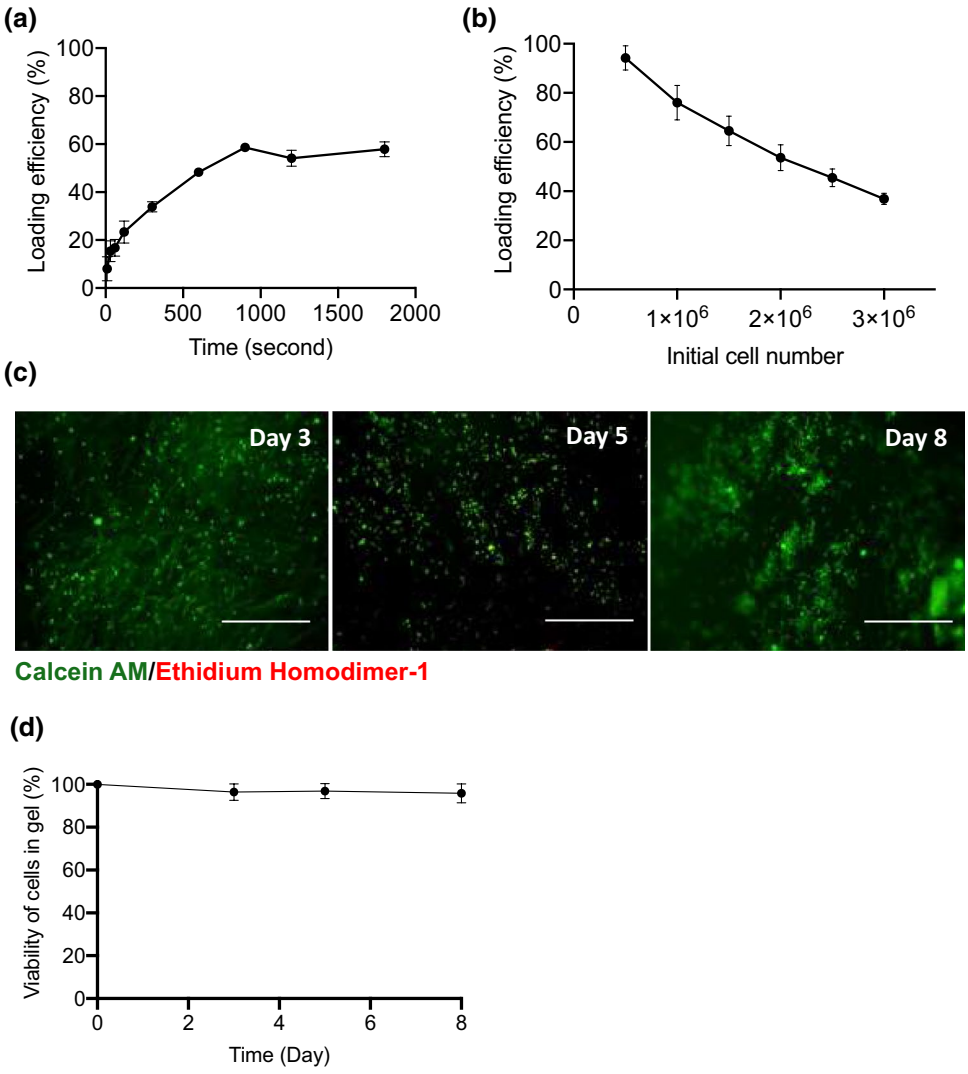

Fig. 4 Macroporous hydrogels enable efficient cell loading and support the survival of cells**.** Macroporous gel were half-dried using Kimwipe followed by addition of EL4 cells in PBS on the top of gels. Shown are **a** Percentage and **b** number of cells loaded in the macroporous gels. **c** Fluorescence images of cells stained with Calcein AM (live cell stain) and Ethidium Homodimer-1(dead cell stain) at 3, 5, and 8 days, respectively post cell loading. **d** Viability of cells in gels over time. All the numerical data are presented as mean ± SD

within the gel. EVs were isolated from the culture medium of ovalbumin (OVA)-expressing E.G7-OVA cancer cells and purified via centrifugation and size exclusion chromatography. The size and size distribution of EVs was determined by transmission electron microscopy (TEM) and dynamic light scattering (DLS) (Fig S1a-b). The E.G7-OVA derived EVs were then loaded together with bone marrow-derived DCs (BMDCs) into macroporous hydrogels. After 16 h, DCs were collected for antibody staining and flow cytometry analysis. Compared to the control group without EVs, DCs cultured within EV-loaded gels successfully expressed SIINFEKL peptide antigen, the CD8 epitope of OVA, via major histocompatibility complex I (MHC I) (Fig. 5a and b). The expression levels of SIINFEKL increased with the concentration of EVs in the gels (Fig. 5a and b). It is noteworthy that the treatment of DCs with a high dose of EVs also upregulated the expression of CD86 and MHCII, two activation markers of DCs (Fig. 5c–f). These experiments demonstrated that DCs can easily infiltrate into the macroporous hydrogel and process and present EV-encased antigens within the gel.

In Vivo DC Recruitment and Modulation by GM-CSF- and EV-Loaded Gels

After demonstrating that macroporous hydrogels can robustly adhere to tissues, easily load and support the survival of cells, and enable the processing of tumor EVs by DCs within the gel, we next studied whether GM-CSF loaded gels can actively recruit DCs in vivo. To load GM-CSF and E.G7-OVA EVs, macroporous hydrogels were half-dried via Kimwipe paper, followed by the addition of EVs and GM-CSF to the top of gels. C57BL/6 mice were divided into 4 groups: gel loaded with GM-CSF and EVs, gel loaded with EVs alone, gel loaded with GM-CSF alone, or blank gel (n = 5 per group). On day 0, gels were applied subcutaneously by cutting a small incision and attaching the gel to the interior side of the skin (gel had a distance from the incision site) (Fig. 6a). On day 4, gels were harvested for immune cell analysis. At the time of collection, gels remained strongly adhered to the skin and were intact (Fig. S2). Flow cytometry analysis revealed that the vast majority of cells present in the gels were $CD45^+$ immune cells (Fig. 6b). Compared to gels loaded with EVs alone or blank gels, gels containing GM-CSF and EVs or gels containing GM-CSF alone recruited a significantly higher number of $CD11c^+$ DCs (Fig. 6c and d), demonstrating the ability of GM-CSF to mediate the attraction of DCs in vivo. Among the recruited $CD11c^+$ DCs, the percentage of activated DCs (i.e., $CD86^+$ population) was higher in gels loaded with EVs, in comparison with gels without EVs or blank gels (Fig. 6e). Gels containing EVs also managed to yield a higher number of SIINFEKL-presenting DCs than gels without EVs or blank gels (Fig. 6f), demonstrating that the recruited DCs can process EVs and present EV-encased SIINFEKL antigens in situ. The macroporous hydrogel loaded with GM-CSF and EVs also recruited $CD11b^+F4/80^+$ macrophages and

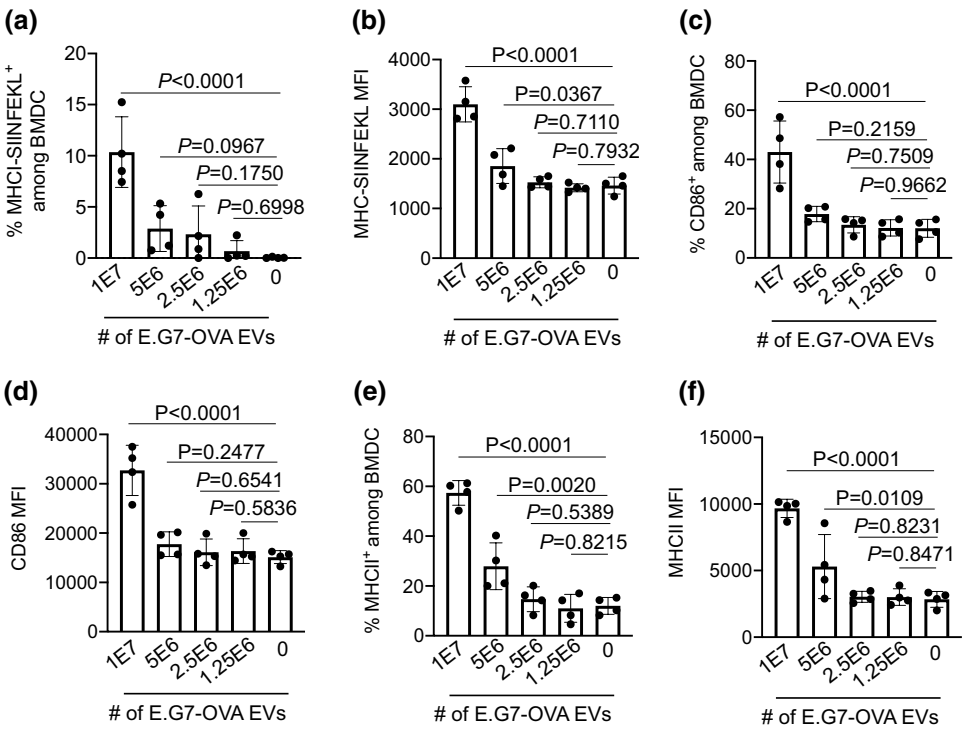

Fig. 5 DCs can process and present tumor EV-encased antigens within macroporous hydrogels. Gels were loaded with DCs and different amounts of E.G7-OVA-derived EVs, and incubated at 37 °C for 16 h. **a** Percentage of MHCI-$SIINFEKL^+$ DCs and **b** mean MHCI-SIINFEKL fluorescence intensity (FI) of DCs after 16 h. **c** Percentage of $CD86^+$ DC and **d** mean CD86 FI of DCs after 16 h. **e** Percentage of $MHCII^+$ DCs and **f** mean MHCII FI of DCs after 16 h. All the numerical data are presented as mean ± SD ($0.01 < {}^*P \le 0.05$; ${}^{**}P \le 0.01$; ${}^{***}P \le 0.001$)

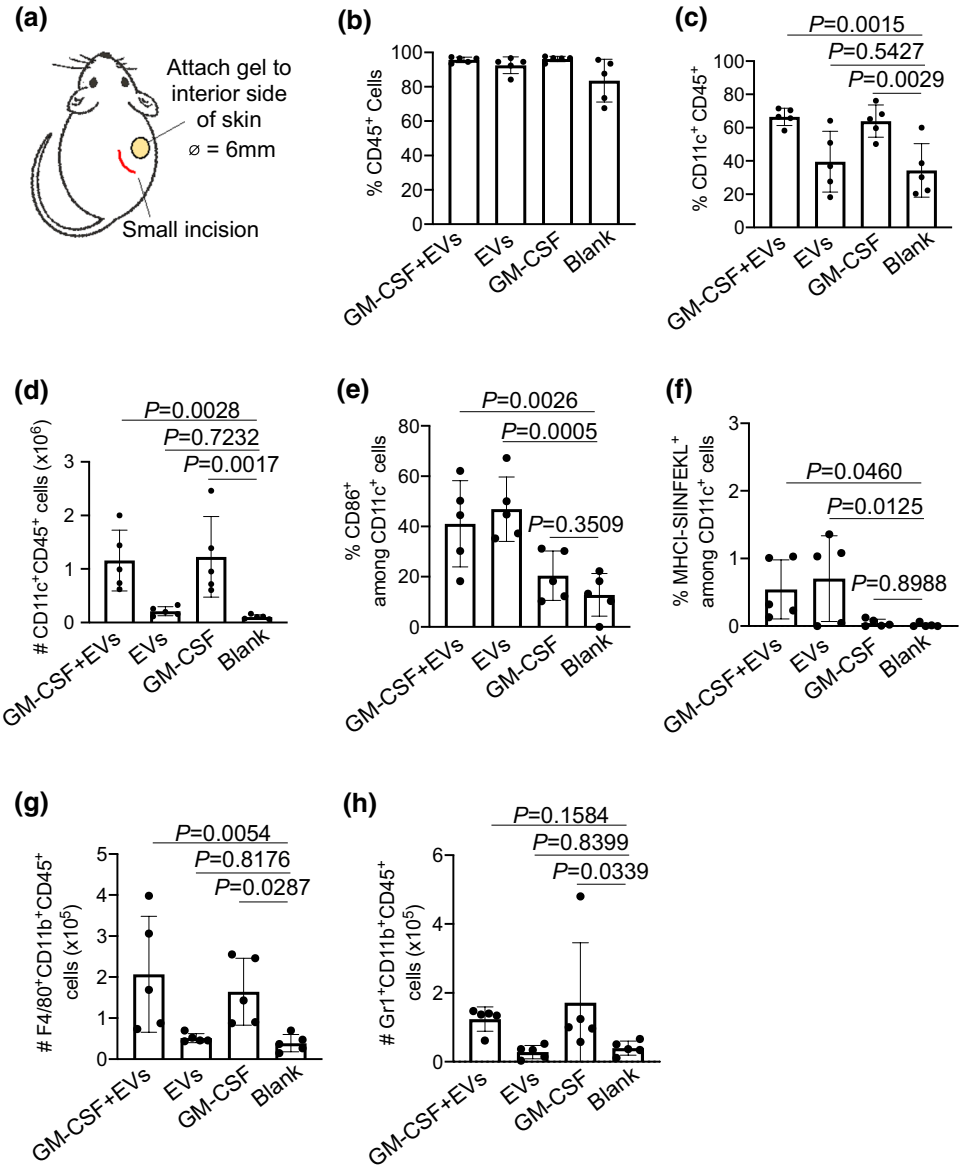

Fig. 6 Macroporous hydrogels loaded with GM-CSF and E.G7-OVA EVs can recruit and modulate DCs in situ. **a** Gel encapsulating E.G7-OVA EVs and GM-CSF, gel encapsulating EVs only, gel encapsulating GM-CSF only, or blank gel were attached to the interior side of mouse back skin through a small incision that had a distance from the gel. Gels were harvested for immune cell analysis after 4 days. **b** Percentage of $CD45^+$ cells among the recruited cells in gels. **c** Percentage of $CD11c^+$ DCs among $CD45^+$ cells and **d** total number of $CD11c^+$ DCs in gels. **e** Percentage of $CD86^+$ cells among $CD11c^+$ cells in gels. **f** Percentage of $MHCI\text{-}SIINFEKL^+$ cells among $CD11c^+$ cells in gels. **g** Number of $CD11b^+F4/80^+$ cells and **h** $CD11b^+Gr\text{-}1^+$ cells in gels. All the numerical data are presented as mean ± SD ($0.01 < {}^*P \le 0.05$; ${}^{**}P \le 0.01$; ${}^{***}P \le 0.001$)

$CD11b^+Gr1^+$ neutrophils, but at a much lower number than DCs (Fig. 6g and h**,** Fig. S3).

CTL Response of GM-CSF- and Tumor EV-Loaded Gels

After demonstrating that bioadhesive macroporous hydrogels loaded with GM-CSF and E.G7-OVA EVs can actively recruit DCs and generate SIINFEKL-presenting DCs in situ, we next studied whether the gel-based cancer vaccine can amplify systemic SIINFEKL-specific CTL response. C57BL/6 mice were divided into five groups: gel loaded with GM-CSF and E.G7-OVA EVs, gel loaded with EVs alone, gel loaded with GM-CSF alone, blank gel, or no treatment (n = 6 per group) (Fig. 7a). Gels were attached to the interior side of mouse back skin on day 0, followed by the analysis of SIINFEKL-specific $CD8^+$ T cells in peripheral blood mononuclear cells (PBMCs) over time. On day 4, a higher number of SIINFEKL $tetramer^+$ $CD8^+$ T cells was detected in mice treated with gels encapsulating GM-CSF and tumor EVs, in comparison with mice treated with blank gels or gels encapsulating GM-CSF alone (Fig. 7b). Upon *ex vivo* restimulation with SIINFEKL peptide, PBMCs collected from mice treated with gels encapsulating GM-CSF and tumor EVs also showed a higher frequency of IFN-γ^+ $CD8^+$ T cells (Fig. 7c). A similar trend, i.e., a higher frequency of SIINFEKL-specific $CD8^+$ T cells in mice treated with gels encapsulating GM-CSF and tumor EVs than mice treated with the blank gel, was also observed on day 8 (Fig. 7d and e). These experiments demonstrated that the bioadhesive macroporous hydrogel loaded with GM-CSF and tumor EVs can generate tumor antigen-presenting DCs

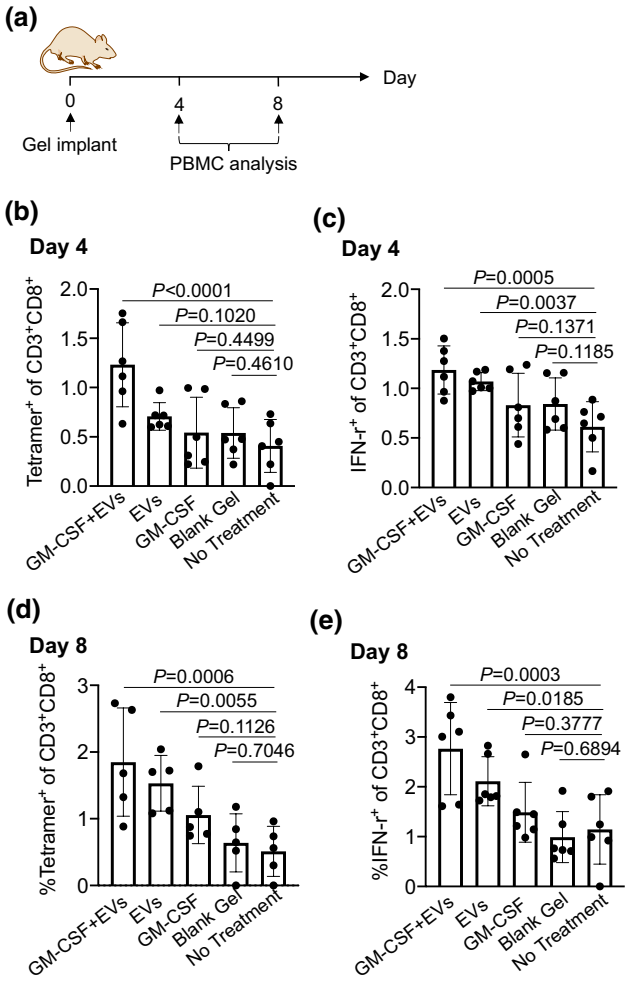

Fig. 7 Macroporous hydrogels loaded with GM-CSF and E.G7-OVA EVs can generate SIINFEKL-specific $CD8^+$ T cell response. **a** Timeline of the vaccination study. Gels loaded with E.G7-OVA EVs and GM-CSF were attached to the interior side of back skin in C57BL/6 mice on day 0, followed by the analysis of SIINFEKL-tetramer$^+$ $CD8^+$ T cells and IFN-γ^+ cells (upon ex vivo SIINFEKL re-stimulation) among $CD8^+$ T cells in PMBCs on day 4 and day 8. Shown are the percentage of **b**, **d** SIINFEKL tetramer$^+$ cells and **c**, **e** IFN-γ^+ cells among $CD8^+$ T cells in PMBC on day 4 and day 8, respectively. All the numerical data are presented as mean ± SD ($0.01 < {*}P \le 0.05$; ${**}P \le 0.01$; ${***}P \le 0.001$)

in situ and these DCs can migrate to lymphatic tissues to prime antigen-specific $CD8^+$ T cells.

Discussion

Macroporous hydrogels that can well retain in the body and enable long-term recruitment and modulation of immune cells (e.g., DCs) hold tremendous promise for the development of robust immunotherapies [4, 9, 46, 47]. Here we introduce a new type of macroporous hydrogel that has superior mechanic strength, supports the infiltration and proliferation of cells within the macropores of the gel, and strongly adhere to tissues upon administration. The macropores were introduced via a cryo-polymerization process where the polymerization of acrylic acid NHS ester, GelMA, and acrylic acid occurs in a frozen state. After forming the gel network and allowing the ice crystals to melt at ambient temperature, gels with a macroporous structure were successfully synthesized [25]. The highly-crosslinked and intertwined double network of gelatin and polyacrylic acid confers a high mechanical strength to the formed gel (~ 1.4 MPa elastic modulus), despite the presence of macropores (~ 80–90 μm in diameter) within the gel network (Fig. 2b–e). It is noteworthy that the macropore size and porosity can be tuned by adjusting the duration of UV irradiation during the polymerization process (Fig. 2b–e). By increasing the UV irradiation time, a tighter gel network can be formed, resulting in a smaller average macropore size and porosity. The presence of hydrophilic polyacrylic acids within the gel network favors the penetration of a high number of water molecules, as evidenced by the high swelling ratio of the macroporous hydrogel (Fig. 2f). The swollen gel network could further facilitate the infiltration of immune cells including DCs in vitro and in vivo.

The incorporation of NHS moieties also allows the gel to covalently conjugate to amine-bearing tissues via amine-NHS chemistry. As the tough gel network can rapidly dissipate the energy from the interface, a stable adhesion layer can be formed between the gel and the tissue such as skin (Fig. 3a–i). The much higher adhesion energy, tensile strength, and shear strength than the commercial sealant Dermabond attested to the superior adhesive property of the macroporous hydrogel (Fig. 3a–i). The adhesive property will allow for the attachment of the gel to different tissues for long-term immunomodulation, hemostasis, drug delivery, among many other applications. In this study, we demonstrated the ability of the macroporous hydrogel to adhere to the interior side of mouse back skin for in situ recruitment and modulation of DCs. By encapsulating GM-CSF into the gel, the gradient of GM-CSF at the gel site enabled the active attraction of DCs in situ (Fig. 6a–e). DCs that arrives at the gel site can easily infiltrate into the macropores of the gel. While we purely rely on the diffusion mechanism to control the release of GM-CSF from gels in this study, further tuning of the release kinetics of GM-CSF in future efforts could lead to the improved recruitment of DCs.

Tumor EVs are a more benign source of tumor antigens than inactivated tumor cells or tumor lysates, and have been actively explored for the development of therapeutic cancer vaccines in preclinical studies and clinical trials [22, 40, 49]. However, the amount of tumor associated antigens encased by the nanosized EVs could be minimal, which is supported by our antigen presentation assay where only a high number of E.G7-OVA-derived EVs

were able to induce the presentation of SIINFEKL antigen by DCs (Fig. 5a and b). This could partially explain the limited antitumor efficacy of conventional tumor EVs vaccines. In order to further improve the antigen presentation process and the overall CTL response, strategies that enable the enhanced uptake and processing of EVs by DCs are needed. In our strategy, by encapsulating tumor EVs into the DC-recruiting macroporous hydrogel, the EVs can be processed by a high number of DCs that are recruited to the gel, resulting in the efficient presentation of EV-encased antigens by DCs in situ (Fig. 6f). These DCs can then traffic to lymphatic tissues to prime antigen-specific $CD8^+$ T cells. We have demonstrated the promise of GM-CSF- and E.G7-OVA EV-loaded macroporous hydrogels to elicit SIINFEKL-specific CTL response (Fig. 7). SIINFEKL-specific $CD8^+$ T cells in PBMCs were detected from day 4, which is consistent with previous reports on macroporous material-based cancer vaccines [27, 45, 48]. The resultant CTL response and antitumor efficacy can be further enhanced by incorporating DC-activating adjuvants and cytokines. The combination of macroporous hydrogel-based EV vaccines with existing immunotherapies such as checkpoint blockades and CAR T therapies will also lead to enhanced efficacy against various types of tumors. [15, 31]

Conclusion

To summarize, we have developed a new bioadhesive macroporous hydrogel that enables in situ recruitment and modulation of DCs. These hydrogels contain macropores that are large enough to home immune cells, and are mechanically tough with an elastic modulus of ~ 1.4 MPa. Due to the presence of NHS moieties, the gel can covalently conjugate to amine-bearing tissues and form a robust adhesion layer with the assistance from the energy-dissipating gel network. By encapsulating GM-CSF into the gel and attaching the gel to mouse skin, a number of DCs can be recruited in situ. We further demonstrated that the recruited DCs can process tumor EVs preloaded in the gel and present EV-encased antigens via MHC complexes, and subsequently mediate the priming of antigen-specific $CD8^+$ T cells. Our bioadhesive macroporous hydrogel system provides a platform for recruiting and modulating DCs in situ and developing enhanced immunotherapy including tumor EV vaccines. Its bioadhesive property and high mechanical strength also enable the stable attachment towards tissues for long-term immunomodulation. We also envision the promise of this material system for drug delivery, tissue regeneration, long-term immunosuppression, and many other applications.

Materials and Methods

Materials

Acrylic acid *N*-hydroxysuccinimide ester, acrylic acid, gelatin methacrylate(gelMA), α-ketoglutaric acid, and gelatin were purchased from Sigma-Aldrich (St. Louis, MO, USA) and used without further purification. Porcine back skin tissues for adhesion tests were purchased from Sierra for Medical Science (Whittier, CA, USA). Poly (methyl methacrylate) films with a thickness of 50 µm were purchased from VWR International (Radnor, PA, USA). TEM grids were purchased from Ted Pella (Redding, CA, USA). BSA assay kit was purchased from Sigma (St. Louis, MO, USA). Calcein AM and Ethidium Homodimer 1 were purchased from Thermofisher (Waltham, MA, USA). Fluorescent images were taken with a EVOS microscope (Thermofisher, Waltham, MA, USA). Mechanical tests were performed with Criterion C43.104E (MTS, Eden Prairie, MN). Recombinant murine GM-CSF was purchased from PeproTech, Inc. (Cranbury, NJ, USA). Primary antibodies used in this study, including Alexa Fluor 700-conjugated anti-CD45 (Invitrogen), PE-conjugated anti-CD11b (Invitrogen), PE/Cy7-conjugated anti-CD11c (Invitrogen), PE-conjugated anti-CD86 (Invitrogen), PerCP/Cy5.5-conjugated anti-F4/80 (Invitrogen), FITC-conjugated anti-Gr-1 (Invitrogen), fluorescein isothiocyanate (FITC)-conjugated anti-CD3-ε (Invitrogen), PE-conjugated anti-CD8-α (Invitrogen), and FITC-conjugated anti-MHCII (Invitrogen), were purchased from Thermo Fisher Scientific (Waltham, MA, USA). Fixable viability dye efluor780 was obtained from Thermo Fisher Scientific (Waltham, MA, USA). All antibodies were diluted according to the manufacturer's recommendations. FACS analyses were collected on Attune NxT flow cytometers and analyzed on FCS Express v6 and v7. Statistical testing was performed using GraphPad Prism v8. Transmission electron microscopic images of EVs were taken with a JEOL 2100. The size and size distribution of EVs were measured with dynamic light scattering (DLS).

Cell Line and Animals

The EL4 and E.G7-OVA cell lines were purchased from American Type Culture Collection (Manassas, VA, USA). Cells were cultured in RPMI 1640 containing 10% FBS, and 100 units/mL Penicillin/streptomycin (with 50 µg/mL G418 for E.G7-OVA cells) at 37 °C in 5% CO_2 humidified air. Female C57BL/6 mice were purchased from Jackson Laboratory (Bar Harbor, ME, USA). Feed and water were available ad libitum. Artificial light was provided in

a 12/12 h cycle. The animal study protocol was reviewed and approved by the Illinois Institutional Animal Care and Use Committee (IACUC) of University of Illinois at Urbana-Champaign.

Preparation of Macroporous Gelatin Hydrogels

A mixture consisting of 30% (w/w) acrylic acid, 10% (w/w) gelatin, 1% (w/w) acrylic acid *N*-hydroxysuccinimde ester, 0.1% (w/w) gelMA, and 0.2% (w/w) α-ketoglutaric acid was dissolved in deionized water. The solution was poured into a PTFE mold and then frozen at − 80 °C for 1 h. The fully frozen mixture was cured under ultraviolet light (320 nm, 40 W power) for 10 minutes.

Porosity Measurement

Macroporous gels were soaked in 1 mL of deionized water at ambient conditions for a few hours. A gel wicking assay was performed using an absorbent Kimwipe (Kimberly-Clark) that touched only one side of the gel, allowing the water within the pores to be drawn out by capillary force. The initial weight of the gel (W_i) and the final weight after the wicking assay (W_f) were measured. The porosity was then calculated as 100% * $(W_i - W_f)/W_i$.

Pore Size Measurement

Macroporous hydrogels were immersed in PBS and examined under an optical microscope. A minimum of 50 images were taken from various regions of the hydrogels. The pore size was measured in each image using ImageJ and the results were averaged. These averages were then calculated over at least 50 images to determine the average pore size of the macroporous hydrogels.

Gel Elastic Modulus Measurement

The modulus of elasticity of the NHS-bearing macroporous hydrogels was determined by performing a compression test. Hydrogels with a dimension of 25 mm × 25 mm × 250 µm (W × L × H) were fully hydrated with deionized water and placed on top of a mold with a 15 mm hole. The gel was firmly clamped onto the mold and a rod with a diameter of 10 mm was used to push down the gel for 12 mm on a mechanical testing machine (Electroforce 3200). The modulus of elasticity was calculated using the following equation:

$$W_{max} = 0.0242\frac{Pa^2}{Eh^3}$$

where W_{max} is the maximum deflection, P is the pressure applied, a is the diameter of the gel, and h is the thickness of the gel.

Adhesion Tests

Porcine tissues were preserved using 0.01% (w/v) sodium azide solution to prevent degradation. 50 µm poly(methylmethacrylate) films were attached to the tissues using cyanoacrylate glue as a backing to prevent tissue stretching. After washing the tissues with PBS, a gelatin gel was applied to the tissue and pressed at 1 kPa for 5 se. The samples were then stored in a wet environment for 24 h to reach swelling equilibrium. The interfacial toughness of the gel was measured using a peeling test. L-shaped aluminum fixtures were attached to polycarbonate sheets with cyanoacrylate glue to guide the peeling test. The specimen was pulled at a constant speed of 50 mm/min using an Electromechanical test frame (CRITERION C43.104E Tall Dual Column 10 kN Frame) with a 200N load cell. The interfacial toughness was calculated by dividing two times the maximum force measured by the sample width. The shear strength was measured using a standard lab-shear test (ASTM D5868) with a 200N load cell. A lap-shear test was conducted at a 50 mm/min peeling speed, and the shear strength was calculated by dividing the maximum force by the adhesion area. The tensile strength was measured using a standard tensile test (ASTM D897) with a 200N load cell. The tensile test was conducted at a 50 mm/min peeling speed, and the tensile strength was calculated by dividing the maximum force by the adhesion area. Porcine back skins were attached to T-shaped aluminum fixtures using cyanoacrylate glue to provide grip for the measurement.

In Vitro Antigen Presentation by DCs

Gels loaded with tumor-derived EVs were placed in 24-well plate. After the gels were partially dried, 10 µL of medium containing BMDCs was added on top of the gels. 1 mL of fresh medium was then added after 15 minutes. After 16 h, the cells in both the gel and the medium were collected and stained with APC-conjugated anti-MHCI-SIINFEKL, PE/Cy7-conjugated anti-CD11c, PE-conjugated anti-CD86, FITC-conjugated anti-MHCII, and the fixable viability dye efluor780 for 20 minutes prior to flow cytometry analysis.

In Situ Immune Cell Recruitment of Gels

C57BL/6 mice were divided into 4 groups: gel with EVs (1×10^7/gel) + GM-CSF (2 µg/gel), gel with EVs (1×10^7/gel), gel with GM-CSF (2 µg/gel), and blank gel (n = 5 per group). On day 0, gels were freshly prepared and subcutaneously implanted into the upper right flank of C56BL/6 mice

(one gel per mouse). Gels were implanted 20 mm away from the incision site to minimize the impact of inflammation at the incision site on the immunomodulatory effect of gels. On day 3, gels were harvested from mice and disrupted using a syringe plunger, releasing contained cells. Cells were pelleted, washed, and stained for flow cytometry analysis. For DC analysis, cells were stained with Alexa Fluor 700-conjugated anti-CD45, PE-conjugated anti-CD11b, PE/Cy7-conjugated anti-CD11c, PE-conjugated anti-CD86 for 20 min. For neutrophil and macrophage analysis, cells were stained with Alexa Fluor 700-conjugated anti-CD45, PE-conjugated anti-CD11b, PerCP/Cy5.5-conjugated anti-F4/80, and FITC-conjugated anti-Gr-1.

Isolation of E.G7-OVA Derived EVs

E.G7-OVA cells were cultured in T75 flasks for 3-4 days. Cell culture medium containing the secreted EVs was collected and concentrated via ultracentrifugation with an Amicon centrifugal filter (100 kDa). EVs were washed with PBS three times and resuspended in PBS. To further purify EVs, a solution of EVs was passed through the qEV size exclusion column. The size and concentration of EVs were determined via Dynamic light scattering and Nanoparticle Tracking Analysis (NTA).

TEM Imaging of EVs

The isolated EVs were carefully placed onto formvar/carbon-coated TEM grids followed by drying and negative staining with 2% aqueous uranyl acetate. The prepared samples were imaged with a JEOL 2100 at 200 kV.

In Vivo Vaccination Study of EV-Loaded Macroporous Gels

C57BL/6 mice were divided into 5 groups: gel with EVs + GM-CSF, gel with EVs, gel with GM-CSF, blank gel, and untreated (n = 6 per group). Gel with EVs + GM-CSF was implanted in mice through a small incision, along with the other groups on Day 0. Blood was drawn on day 4 and 8, respectively for analysis of SIINFEKL-specific $CD8^+$ T cells via tetramer stain or IFN-γ restimulation. For tetramer analysis, PBMCs were stained with APC-conjugated SIINFEKL tetramer, FITC-conjugated anti-CD3, PE-conjugated anti-CD8, and e780 fixable viability dye for 20 min prior to FACS assay. For IFN-γ restimulation, PBMCs were stimulated with SIINFEKL peptide for 1.5 h, treated with Golgi plug for 2.5 h, stained with FITC-conjugated anti-CD3, PE-conjugated anti-CD8, and e780 fixable viability dye, treated with the fixation & permeabilization buffer, and stained with APC-conjugated anti-IFN-γ, prior to FACS assay. In the following prophylactic tumor study, E.G7-OVA tumor cells (0.1 million cells in 50 μL of HBSS) were subcutaneously injected into the upper flank of C57BL/6 mice on day 9. The tumor volume of mice was measured every 3 days. The tumor volume was calculated using the formula $(\text{length}) \times (\text{width})^2/2$, where the long axis diameter was regarded as the length and the short axis diameter was regarded as the width.

Statistical Analyses

Statistical analysis was performed using GraphPad Prism v6 and v8. Sample variance was tested using the F test. For samples with equal variance, the significance between the groups was analyzed by a two-tailed student's t-test. For samples with unequal variance, a two-tailed Welch's t-test was performed. For multiple comparisons, a one-way analysis of variance (ANOVA) with post hoc Fisher's LSD test was used. The results were deemed significant at $0.01 < *P \leq 0.05$, highly significant at $0.001 < **P \leq 0.01$, and extremely significant at $***P \leq 0.001$.

Supplementary Information The online version contains supplementary material available at https://doi.org/10.1007/s12195-023-00770-2.

Acknowledgements The authors would like to acknowledge the financial support from NSF DMR 2143673 CAR, NSF GCR 2121003, R01CA274738, NIH R21CA270872, and the start-up package from the Department of Materials Science and Engineering at the University of Illinois at Urbana-Champaign and the Cancer Center at Illinois. Han J. acknowledges the support from the Cancer Scholars for Translational and Applied Research (C*STAR) Program (CST EP082021). Bhatta R. acknowledges the support from the National Institute of Biomedical Imaging and Bioengineering of the National Institutes of Health (T32EB019944).

Data Availability Raw data can be accessed upon request, and will be published upon the acceptance of the manuscript.

Declarations

Conflict of interest The authors (Joonsu Han, Rimsha Bhatta, and Hua Wang) declare no competing financial interests.

Ethics Approval This paper does not involve any research of human subjects. For studies involving mice, the ethical principles established by the National Institutes of Health Guide for the Care and Use of Laboratory Animals (NIH Publications No. 8523, revised 2011) were followed.

References

1. Ali, O. A., N. Huebsch, L. Cao, G. Dranoff, and D. J. Mooney. Infection-mimicking materials to program dendritic cells in situ. *Nat. Mater.* 8:151–158, 2009.
2. Allen, R., E. Ivtchenko, B. Thuamsang, R. Sangsuwan, and J. S. Lewis. Polymer-loaded hydrogels serve as depots for lactate and mimic "cold" tumor microenvironments. *Biomater. Sci.* 8:6056–6068, 2020.

3. Bencherif, S. A., et al. Injectable cryogel-based whole-cell cancer vaccines. *Nat. Commun.* 6:7556, 2015.
4. Bhatta, R., J. Han, Y. Liu, Y. Bo, and H. Wang. T cell-responsive macroporous hydrogels for in situ T cell expansion and enhanced antitumor efficacy. *Biomaterials*.293:121972, 2023.
5. Blacklow, S. O., et al. Bioinspired mechanically active adhesive dressings to accelerate wound closure. *Sci. Adv.* 5:e3963, 2019.
6. Blass, E., and P. A. Ott. Advances in the development of personalized neoantigen-based therapeutic cancer vaccines. *Nat. Rev. Clin. Oncol.* 18:215–229, 2021.
7. Cai, L., et al. Engineered biomaterials for cancer immunotherapy. *MedComm.* 1:35–46, 2020.
8. Callmann, C. E., et al. Tumor cell lysate-loaded immunostimulatory spherical nucleic acids as therapeutics for triple-negative breast cancer. *Proc. National Acad. Sci.* 117:17543–17550, 2020.
9. Calmeiro, J., et al. Biomaterial-based platforms for in situ dendritic cell programming and their use in antitumor immunotherapy. *J. Immunother. Cancer.* 7:238, 2019.
10. Couzin-Frankel, J. Cancer immunotherapy. *Science*. 342:1432–1433, 2013.
11. Dellacherie, M. O., et al. Single-shot mesoporous silica rods scaffold for induction of humoral responses against small antigens. *Adv. Funct. Mater.* 30:2002448, 2020.
12. Donlon, N. E., R. Power, C. Hayes, J. V. Reynolds, and J. Lysaght. Radiotherapy, immunotherapy, and the tumour microenvironment: turning an immunosuppressive milieu into a therapeutic opportunity. *Cancer Lett.* 502:84–96, 2021.
13. Eso, Y., T. Shimizu, H. Takeda, A. Takai, and H. Marusawa. Microsatellite instability and immune checkpoint inhibitors: toward precision medicine against gastrointestinal and hepatobiliary cancers. *J. Gastroenterol.* 55:15–26, 2020.
14. Gan, D., et al. Plant-inspired adhesive and tough hydrogel based on Ag-Lignin nanoparticles-triggered dynamic redox catechol chemistry. *Nat. Commun.* 10:1487, 2019.
15. Grosskopf, A. K., et al. Delivery of CAR-T cells in a transient injectable stimulatory hydrogel niche improves treatment of solid tumors. *Sci. Adv.* 8:8264, 2022.
16. Hammerstrom, A. E., D. H. Cauley, B. J. Atkinson, and P. Sharma. Cancer immunotherapy: Sipuleucel-T and beyond. *Pharmacotherapy*. 31:813–828, 2011.
17. Han, J., et al. A double crosslinking adhesion mechanism for developing tough hydrogel adhesives. *Acta Biomater.* 150:199–210, 2022.
18. Han, J., R. Bhatta, Y. Liu, Y. Bo, and H. Wang. In situ dendritic cell recruitment and T cell activation for cancer immunotherapy. *Front. Pharmacol.* 13:15, 2022.
19. Hegde, P. S., and D. S. Chen. Top 10 challenges in cancer immunotherapy. *Immunity*. 52:17–35, 2020.
20. Hua, Y., et al. Ultrafast, tough, and adhesive hydrogel based on hybrid photocrosslinking for articular cartilage repair in water-filled arthroscopy. *Sci. Adv.* 7:0628, 2021.
21. Huang, Y., et al. Vascular normalizing doses of antiangiogenic treatment reprogram the immunosuppressive tumor microenvironment and enhance immunotherapy. *Proc. Natl. Acad. Sci. USA*. 109:17561–17566, 2012.
22. Huang, L., et al. Engineered exosomes as an in situ DC-primed vaccine to boost antitumor immunity in breast cancer. *Mol. Cancer*. 21:45, 2022.
23. Huang, L., et al. Natural blood plasma-based hydrogels as tumor vaccines delivery systems to enhance biomimetic recruitment of antigen presenting cells for tumor immunotherapy. *Mater. Today Bio*.17:100497, 2022.
24. Kawahara, M., and H. Takaku. A tumor lysate is an effective vaccine antigen for the stimulation of CD4+ T-cell function and subsequent induction of antitumor immunity mediated by CD8+ T cells. *Cancer Biol. Ther.* 16:1616–1625, 2015.
25. Lei, L., et al. Hydrogel-guided strategies to stimulate an effective immune response for vaccine-based cancer immunotherapy. *Sci. Adv.* 8:8738, 2022.
26. Lesterhuis, W. J., J. B. A. G. Haanen, and C. J. A. Punt. Cancer immunotherapy – revisited. *Nat. Rev. Drug Discov.* 10:591–600, 2011.
27. Li, A. W., M. C. Sobral, S. Badrinath, et al. A facile approach to enhance antigen response for personalized cancer vaccination. *Nat. Mater.* 17:528–534, 2018.
28. Liu, Y., et al. In situ modulation of dendritic cells by injectable thermosensitive hydrogels for cancer vaccines in mice. *Biomacromolecules*. 15:3836–3845, 2014.
29. Liu, C., et al. A nanovaccine for antigen self-presentation and immunosuppression reversal as a personalized cancer immunotherapy strategy. *Nat. Nanotechnol.* 17:531–540, 2022.
30. Liu, Y., et al. Injectable hydrogel as a unique platform for antitumor therapy targeting immunosuppressive tumor microenvironment. *Front Immunol.*12:832942, 2022.
31. Liu, M., Z. Cao, R. Zhang, Y. Chen, and X. Yang. Injectable Supramolecular hydrogel for locoregional immune checkpoint blockade and enhanced cancer chemo-immunotherapy. *ACS Appl. Mater. Interfaces*. 13:33874–33884, 2021.
32. Makkouk, A., and G. J. Weiner. Cancer immunotherapy and breaking immune tolerance: new approaches to an old challenge. *Cancer Res.* 75:5–10, 2015.
33. Martin, J. D., H. Cabral, T. Stylianopoulos, and R. K. Jain. Improving cancer immunotherapy using nanomedicines: progress, opportunities and challenges. *Nat. Rev. Clin. Oncol.* 17:251–266, 2020.
34. Mellman, I., G. Coukos, and G. Dranoff. Cancer immunotherapy comes of age. *Nature*. 480:480–489, 2011.
35. Naseri, M., M. Bozorgmehr, M. Zöller, E. Ranaei-Pirmardan, and Z. Madjd. Tumor-derived exosomes: the next generation of promising cell-free vaccines in cancer immunotherapy. *Oncoimmunology*. 9:1779991, 2020.
36. Palucka, K., and J. Banchereau. Dendritic-cell-based therapeutic cancer vaccines. *Immunity*. 39:38–48, 2013.
37. Peng, M., et al. Neoantigen vaccine: an emerging tumor immunotherapy. *Mol. Cancer*. 18:128, 2019.
38. Phuengkham, H., L. Ren, I. W. Shin, and Y. T. Lim. Nanoengineered immune niches for reprogramming the immunosuppressive tumor microenvironment and enhancing cancer immunotherapy. *Adv. Mater.* 31:1803322, 2019.
39. Rezaie, J., M. Feghhi, and T. Etemadi. A review on exosomes application in clinical trials: perspective, questions, and challenges. *Cell Commun. Signal.* 20:145, 2022.
40. Santos, P., and F. Almeida. Exosome-based vaccines: history, current state, and clinical trials. *Front. Immunol.* 12:48, 2021.
41. Sun, J.-Y., et al. Highly stretchable and tough hydrogels. *Nature*. 489:133–136, 2012.
42. Sutherland, S. I. M., X. Ju, L. G. Horvath, and G. J. Clark. Moving on from sipuleucel-T: new dendritic cell vaccine strategies for prostate cancer. *Front. Immunol.* 12:89, 2021.
43. Thakur, A., D. C. Parra, P. Motallebnejad, M. Brocchi, and H. J. Chen. Exosomes: Small vesicles with big roles in cancer, vaccine development, and therapeutics. *Bioactive Mater.* 10:281–294, 2022.
44. Verbeke, C. S., and D. J. Mooney. Injectable, pore-forming hydrogels for in vivo enrichment of immature dendritic cells. *Adv. Healthc. Mater.* 4:2677–2687, 2015.
45. Wang, H., et al. Metabolic labeling and targeted modulation of dendritic cells. *Nat. Mater.* 19:1244–1252, 2020.
46. Wang, H. Immune cell homing biomaterials for immunotherapy. *Acc. Mater. Res.* 1:172–174, 2020.

47. Wang, H., and D. J. Mooney. Biomaterial-assisted targeted modulation of immune cells in cancer treatment. *Nat. Mater.* 17:761–772, 2018.
48. Wang, H., A. J. Najibi, M. C. Sobral, et al. Biomaterial-based scaffold for in situ chemo-immunotherapy to treat poorly immunogenic tumors. *Nat. Commun.* 11:5696, 2020.
49. Xu, Z., S. Zeng, Z. Gong, and Y. Yan. Exosome-based immunotherapy: a promising approach for cancer treatment. *Mol. Cancer*. 19:160, 2020.
50. Yuk, H., et al. Dry double-sided tape for adhesion of wet tissues and devices. *Nature*. 575:169–174, 2019.
51. Zhang, Z., et al. Neoantigen: a new breakthrough in tumor immunotherapy. *Front. Immunol.* 12:59, 2021.
52. Ziemba, A. M., et al. Stabilized interleukin-4-loaded poly(lactic-co-glycolic) acid films shift proinflammatory macrophages toward a regenerative phenotype in vitro. *ACS Appl. Bio. Mater.* 2:1498–1508, 2019.

Authors and Affiliations

Joonsu Han[1] · Rimsha Bhatta[1] · Hua Wang[1,2,3,4,5,6,7]

✉ Hua Wang
huawang3@illinois.edu

[1] Department of Materials Science and Engineering, University of Illinois at Urbana-Champaign, Urbana, IL 61801, USA

[2] Cancer Center at Illinois (CCIL), Urbana, IL 61801, USA

[3] Department of Bioengineering, University of Illinois at Urbana-Champaign, Urbana, IL 61801, USA

[4] Carle College of Medicine, University of Illinois at Urbana-Champaign, Urbana, IL 61801, USA

[5] Beckman Institute for Advanced Science and Technology, University of Illinois at Urbana-Champaign, Urbana, IL 61801, USA

[6] Materials Research Laboratory, University of Illinois at Urbana-Champaign, Urbana, IL 61801, USA

[7] Institute for Genomic Biology, University of Illinois at Urbana-Champaign, Urbana, IL 61801, USA